Journal of Power Sources 448 (2020) 227223

Contents lists available at ScienceDirect

Journal of Power Sources

journal homepage: www.elsevier.com/locate/jpowsour

Assessing the potential of molten carbonate fuel cell-based schemes for carbon capture in natural gas-fired combined cycle power plants

M. Spinelli [a,*], D. Di Bona [a], M. Gatti [a,b], E. Martelli [b], F. Viganò [a,b], S. Consonni [a,b]

[a] LEAP s.c.a.r.l, via Nino Bixio 27C, 29121, Piacenza, Italy
[b] Politecnico di Milano, Department of Energy, Via Lambruschini 4, 20156, MI, Italy

HIGHLIGHTS

- Performance of Integrated and Non-integrated MCFC + NGCC schemes are simulated.
- The impact of CO_2 Utilization Factor on plant performance and costs is evaluated.
- Metal dusting influences the heat exchanger network design and process performance.
- MCFC-based configurations are benchmarked against the EBTF NGCC featuring MEA CCS.
- Performances (SPECCA, CCA) and retrofitability of the MCFC schemes are evaluated.

ARTICLE INFO

Keywords:
Post-combustion CO_2 capture
Molten carbonate fuel cell
Natural gas combined cycle
Metal dusting
Cost of CO_2 avoided

ABSTRACT

This work explores two configurations of natural gas-fired combined cycles (NGCC) with molten carbonate fuel cells (MCFC) for CO_2 capture. Special attention is devoted to the selection of MCFC operating conditions (trade-off between CO_2 capture and voltage losses), heat integration scheme, fuel use and CO_2 purification. Two schemes are considered: (i) in the first "integrated" scheme, MCFC modules are installed between the gas turbine and the heat recovery steam generator (HRSG) to maximize the efficiency of the integrated power plant; (ii) in the second "non-integrated" layout, the MCFC is located downstream of the HRSG and a regenerative heat exchanger is designed to preheat cathode reactants up to the MCFC working temperature. This study includes a full techno-economic analysis of the two layouts based on a preliminary sizing of the key-components, and a sensitivity analysis on the CO_2 utilization factor. Compared to a benchmark amine scrubbing process, the "integrated" configuration shows considerably better performance (Specific Primary Energy Consumption for CO_2 Avoided - SPECCA = 0.31 MJ kg_{CO2}^{-1}; Cost of CO_2 avoided - CCA = 50 \$ t_{CO2}^{-1}), whereas the "non-integrated" solution shows higher energy penalties but similar CO_2 avoidance cost (SPECCA = 2.4 MJ kg_{CO2}^{-1}; CCA = 76 \$ t_{CO2}^{-1}).

1. Introduction

The crucial Paris agreement stipulated in 2015 (Conference of Parties, COP21) reinforced the common awareness about serious and long-term - or even permanent - consequences of global warming, and paved a strategic way for joint actions to keep the global temperature increase below 2 °C. It is widely recognized that anthropogenic greenhouse gas (GHG) emissions are mainly responsible for the gradual disruption of our climate system: their mitigation is a critical challenge for all the developed countries, but also an essential goal in the fight against climate change [1–3]. The following negotiations in COP22 (Morocco), COP23 (Germany) and COP24 (Poland) gave some strong inputs to the scientific communities and to the industries involved in the energy sectors, with the aim of pushing the energy-intensive sectors towards carbon neutrality. Nevertheless, all these effort are still too modest if compared to the risks connected with the global temperature rise [4]. A common output of the forecast scenarios developed by IPCC is the importance of carbon capture and storage (CCS) technologies, that should be likely deployed in the set of joint solutions (i.e. penetration of renewable energy sources and low carbon fuels) for reducing net GHG emissions and mitigating the climate change in the near future [2]. The benchmark technology for post-combustion CCS in natural gas-fired power plants is chemical absorption with amine-based solvents [5]. However, the high investment cost and energy penalty of amine scrubbing processes hinders their utilization for CCS. Among the most

* Corresponding author.
E-mail address: maurizio.spinelli@polimi.it (M. Spinelli).

https://doi.org/10.1016/j.jpowsour.2019.227223
Received 23 July 2019; Received in revised form 26 September 2019; Accepted 27 September 2019
Available online 22 November 2019
0378-7753/© 2019 The Authors. Published by Elsevier B.V. This is an open access article under the CC BY license (http://creativecommons.org/licenses/by/4.0/).

Nomenclature

CCA	Cost of CO_2 avoided [\$ $t_{CO2\text{-}1}$]
CCP	CO_2 Capture Project
CCR	Carbon Capture Rate
CCS	Carbon Capture & Storage
CHP	Combined Heat and Power
COE	Cost of Electricity [\$ MWh_{el}^{-1}]
COP	Conference of Parties
DIR	Direct Internal Reforming
e	Specific Emissions [kg_{CO2} MWh_{el}^{-1}]
EBTF	European Benchmarking Task Force
ECO	Economizer
EOR	Enhanced Oil Recovery
EPC	Engineering, Procurement and Construction
EVA	Evaporator
FCE	Fuel Cell Energy Inc.
GHG	Greenhouse gas
GPU	Gas Processing Unit
GT	Gas Turbine
HEX	Heat Exchanger
HRSC	Heat Recovery Steam Cycle
HRSG	Heat Recovery Steam Generator
IC	Current density [A m^{-2}]
IIR	Indirect Internal Reforming
LMTD	Logaritmic Mean Temperature Difference
LP	Low Pressure
MCFC	Molten Carbonate Fuel Cell
MEA	MonoEthanolAmine
MP	Medium Pressure
NG	Natural Gas
NGCC	Natural Gas Combined Cycle
NTU	Number of Transfer Units
O&M	Operation and Maintenance
p	Partial pressure
P	Power [MW]
Q	Thermal power [MW]
S/C	Steam to Carbon ratio
SOFC	Solid Oxide Fuel Cell
SPECCA	Specific Primary Energy Consumption for CO_2 avoided [MJ kg_{CO2}^{-1}]
T	Temperature
TDPC	Total Direct Plant Cost
TEC	Total Equipment Cost
TIT	Turbine Inlet Temperature
TPC	Total Plant Cost
TRL	Technology Readiness Level
U	Utilization Factor
V	Voltage
X	Molar/Volumetric fraction

Greek symbols

β	Gas turbine pressure ratio
ε	Thermal effectiveness
η	Net efficiency
ΔT	Difference of Temperature
$\Delta V_{(Act\text{-}Ohm\text{-}Conc)}$	Activation/ Ohmic /Concentration overpotential

Subscripts

CCS	Carbon Capture & Storage
el	Electric
F	Fuel
LHV	Low Heating Value
ref	Reference
spec	Specific

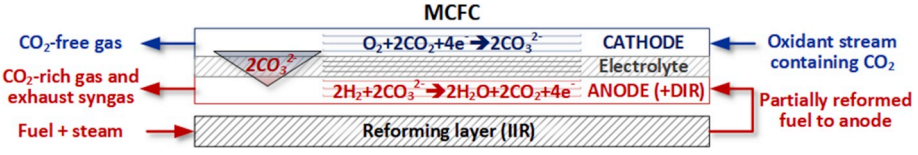

Fig. 1. MCFC working principle and general electrochemical anode/cathode reactions.

promising CCS alternatives, the application of MCFCs for CO_2 capture [6–10] of this capture concept and of the parallel commercial exploitation of MCFC modules is now triggering the development of the first CO_2 capture demonstration projects [11].

According to the recent study [12], the MCFC-based capture system looks promising when compared to amines and other four novel CO_2 capture systems. As conceptually illustrated in Fig. 1, if CO_2-rich flue gas is fed to the fuel cell cathode, the MCFC electrochemical reaction makes possible the CO_2 separation from the cathode stream, and its migration towards the anode (fed with internally reformed fuel) due to the permeation of CO_3^{2-} ions through a liquid carbonate electrolyte retained in a ceramic matrix. Since this operating principle produces an external electrical current flow, the MCFC allows the separation of CO_2 from the NGCC flue gas while simultaneously generating additional electric power with high electric efficiency. The concept of exploiting the favourable ion transport to separate CO_2 from combustion effluents has been extensively studied for CCS applications to several power and industrial sectors. As a general outcome, this system is able to achieve high CO_2 capture rates (up to 80–90%) and high electric efficiencies, but their value depends on the specific application. Indeed MCFC performances are influenced by the CO_2 concentration in the combustion effluents fed to the MCFC cathode [13], which is characterized by a wide range of variability (4–30 mol%) depending on the source process.

The schematic of a MCFC fed with natural gas is shown in Fig. 1. The key components of the fuel cell are the two electrodes, made of nickel-based alloys (e.g., Ni–Al–Cr) at the anode and high porosity oxides (NiO–MgO) at the cathode, and a liquid carbonate electrolyte retained in a ceramic matrix capable of transporting CO_3^{2-} ions [14]. CO_2-rich flue gas is fed to the fuel cell cathode while a mixture of natural gas and steam is fed to the anode side. Natural gas is converted to hydrogen by a first *indirect* internal reforming process (IIR, obtained in a proper layer interposed through two different MCFC active layers) and a second *direct* reforming process (DIR) occurring inside the MCFC anode and driven by the progressive H_2 consumption.

MCFC-based CCS layouts have been proposed in the power sector for retrofitting coal- and NG-fired power plants and for greenfield integrated applications, showing promising results according to the most recent modelling studies. Examples include natural gas combined cycles

(NGCC) [15–18], coal-fired plants [7,10,19], integrated coal gasification combined cycles (IGCC) [20], and biogas plants [21]. More recently, the use of MCFC as CO_2 concentrator has been conceived for several industrial fields: the work [22] explores some downstream options of MCFC modules used in a cement plant to capture the CO_2 generated by combustion and $CaCO_3$ calcination, producing carbon-free power for self-consumptions and for export to the grid. Some patents are dedicated to several MCFC applications designed to capture carbon dioxide from industrial emitting sources, like steel plant [23]. In the study [24] an integrated MCFC plant is designed to capture 90% of the CO_2 from the effluents produced in the steam generator of an oil sands facility, and to produce heat and power for internal use.

As far as NGCCs are concerned, the most efficient way to integrate a NGCC with a MCFC power plant is based on the installation of the fuel cell section between the GT and the HRSG of the combined cycle, as proposed in Ref. [25]. This "integrated" NGCC + MCFC solution is analysed also in Ref. [26], where a synergistic operation of MCFC and membranes is proposed. Due to some technological constraints (i.e. the presence of an external reformer and the stack maximum temperature), the proposed layout features a carbon capture rate of about 60% with the MCFC producing 11% of the total net power output. When the NG reformer is thermally integrated with the MCFC modules (owing to high operating temperatures and to the large availability of nickel surfaces), the endothermic reforming reaction reduces the temperature increase across the MCFC and allows the operation of the fuel cell section with higher CO_2 utilization factors, resulting also in larger MCFC active area and higher power outputs. A comparison between internal and external reforming is investigated in Ref. [17], where a promising NGCC + MCFC configuration features a high carbon capture rate (up to 85%) and a significant increase of the power plant electricity output (+20%) with a specific energy consumption for CO_2 avoided (SPECCA) limited to 0.4 MJ kg_{CO2}^{-1}. The downstream (also named "bolt-on") layout proposed in Ref. [27] explores the post-combustion application of a MCFC island to NGCCs and to pulverized coal fired steam cycles (PCC), as a retrofit to the original power plant. This "non-integrated" layout is more retrofitable, because it minimizes the changes to both the baseline power plant layouts, and yeilds a significant carbon capture rate (>80%) and a very limited (<3%) decrease in efficiency with respect to the baseline NGCC.

The main objective of this work is to provide a comprehensive comparison between the integrated and non-integrated (also named "fully-retrofitable") NGCC + MCFC solutions, assessing the two configurations with the same basis of design. In particular, the techno-economic analysis of both the configurations will take into account:

- the updated polarization curves integrated within a recent 0D MCFC model, which includes indirect and direct internal reforming (IIR and DIR), as described in Ref. [27];
- the effect of the possible metal dusting issues on the design of the heat exchanger network, especially concerning the anode and cathode preheating sections;
- the specific engineering design and cost assessment of some pieces of heat transfer equipment;
- the effect of CO_2 utilization factor on the power plant performance and cost.

The energy and economic performance of the MCFC-based power plants are compared with those of a benchmark amine scrubbing post-combustion processes previously assessed elsewhere [12].

2. MCFC working principle, layouts and modelling

The performance of a MCFC depends on several operating parameters: the working temperature and pressure, the current density (i.e., electric current per unit of active electrolyte area), the composition of the feed streams (anode and cathode) and the excess of reactants fed to

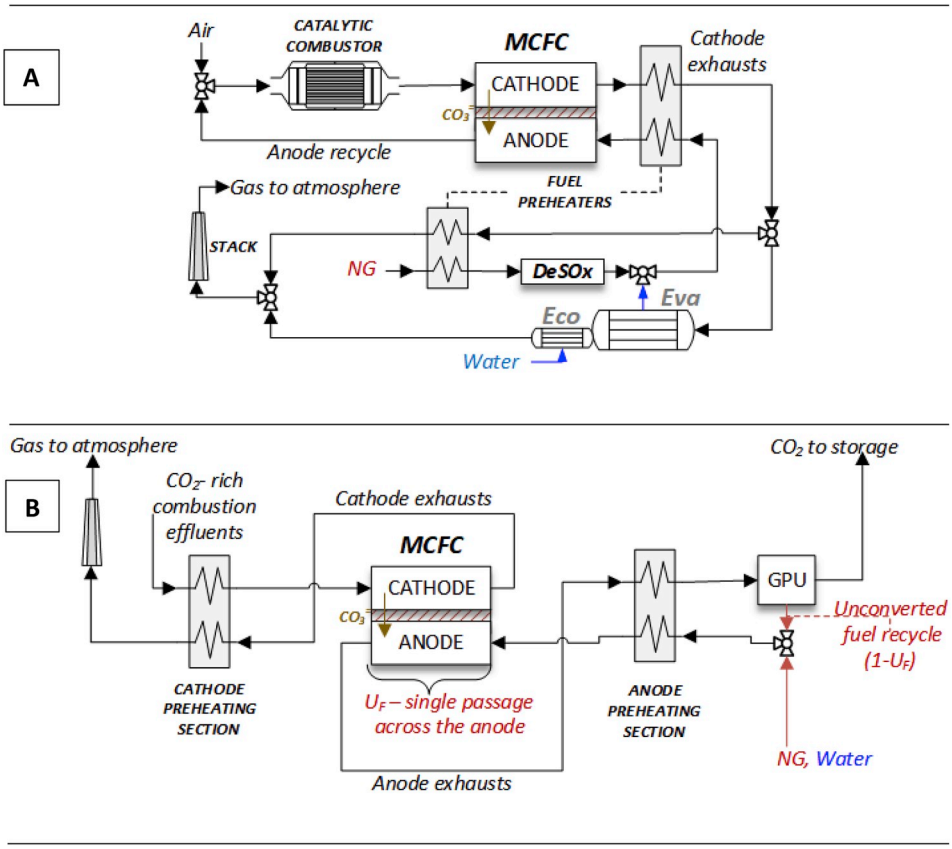

Fig. 2. Simplified layout of the MCFC stand alone (A) and carbon capture (B) application. In case A, the source for the CO_2 fed to the cathode is the anode effluent coming from the fuel cell itself (internal recycle anode → cathode). Before being introduced to the cathode, the unconverted syngas contained in anode exhausts is oxidized in a catalytic combustor. Cathode effluents are exploited for preheating natural gas and for preheating water in the economizer (ECO) and raising LP steam in the evaporator (EVA). The carbon capture layout of case B shows that, owing to the gas processing unit which separates the unconverted fuel (or exhaust syngas) from the CO_2 stream leaving the anode, the fraction ($1-U_F$) can be recycled to the anode inlet, bringing the overall fuel utilization close to 100%.

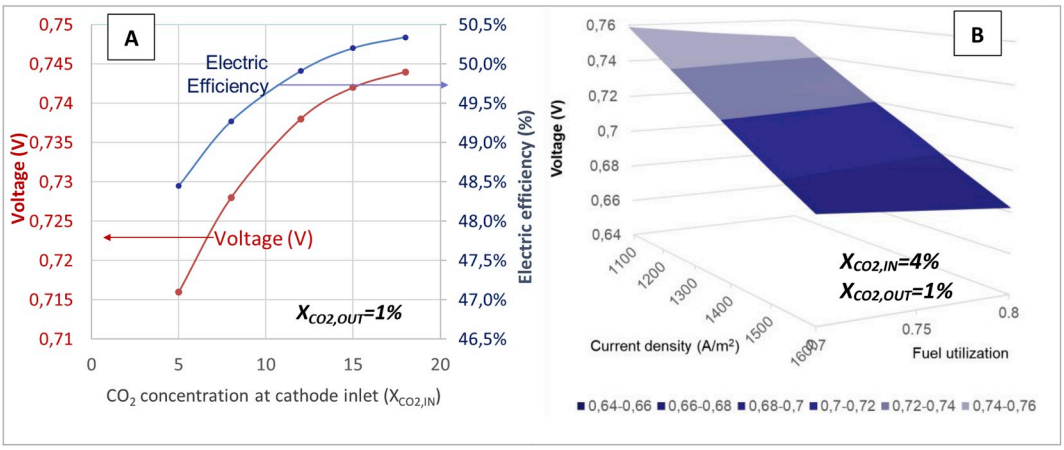

Fig. 3. MCFC voltage and gross efficiency variation as a function of CO_2 concentration at the cathode inlet (A - left side) and as a function of current density/fuel utilization (B - right side). Operating conditions: cathode/anode streams inlet temperature 580 °C; cathode/anode streams inlet pressure 1.05/1.10 bar.

the fuel cell with respect to the minimum stoichiometric requirement. Typically, in place of the excess of reactants, the utilization factors (denoted with U_{O2}, U_{CO2}, U_{H2}) are adopted as design parameters: they are defined as the fraction of O_2, CO_2, H_2 effectively consumed by the reaction with respect to the total amount fed to the MCFC.

Various 0-D modelling approaches have been proposed in the literature to analyze MCFC performance, spanning from more detailed reduced order models requiring several experimental data for calibration [28] to simplified linearized models [29] used for optimization and off-design analysis. In this work, the 0-D model presented by Spinelli et al. in Ref. [27] is employed; the model was developed and calibrated against experimental data within the range of CO_2 concentrations (i.e. between natural gas and cement flue gases) and of fuel utilization factors analysed in this work.

The performance of the fuel cell can be modelled using the potential of an ideal fuel cell as reference (E_{Nernst}, also called Nernst potential) and subtracting the voltage losses due to the reaction activation mechanism ΔV_{Act}, the ohmic losses ΔV_{Ohm}, and the non homogenous reactant concentrations ΔV_{Conc} [14]:

$$V = E_{Nernst} - \Delta V_{Act} - \Delta V_{Ohm} - \Delta V_{Conc} \quad (1)$$

E_{Nernst} is related to the Gibbs free energy associated with the electrochemical reaction, corrected with a function of operating temperature and of the partial pressures of the reactants:

$$E_{Nernst} = \frac{\Delta G}{nF} + \frac{RT}{nF}\ln\left(\frac{p_{H_2an}\left(p_{O_2ct}\right)^{0.5} p_{CO_2ct}}{p_{H_2Oan}\, p_{CO_2an}}\right) \quad (2)$$

Since the average partial pressures of all the reactants at the anode (p_{H_2an} and p_{H_2Oan}) and at the cathode (p_{O_2ct},p_{CO_2ct} and p_{H_2Oct}) sides of the MCFC depends on the inlet and outlet streams compositions, the ideal Nernst voltage is significantly influenced by the utilization factors of all the species.

Once the potential V is known, the gross power produced by the MCFC can be calculated as:

$$P_{el,MCFC} = V \cdot IC \cdot A[W] \quad (3)$$

where IC is the current density and A is the active MCFC area.

The voltage (as well as the cell efficiency) depends on the current density IC, reactants inlet concentrations and utilization factors. In order to have a high voltage, the MCFC should operate with low current density (as to limit the ohmic losses) and high inlet reactant concentrations (beneficial for the Nernst potential and concentration losses).

The fuel cell 0D model was implemented in the source code of the GS software [30] and includes:

- equation for coupling mass/energy balances with the MCFC electrochemical reactions;
- calibrated voltage correlations;
- the routines for the simulation of the direct and indirect internal reforming processes (respectively IIR and DIR).

The model allows the user to set the fuel pre-conversion in the pre-reformer layer, and calculates the energy balance of the whole stack, the total current and power produced by the MCFC, and the global active area of the fuel cell stack. The correlation used in this study to estimate the MCFC voltage results from a polarization curve interpolated on the data gathered during an experimental analysis, which was previously carried out internally at Fuel Cell Energy Inc. (FCE) using simulated coal and NG power plant effluents (as discussed in Refs. [12,27]). The correlation allows computing the MCFC voltage as a difference between Nernst potential and all the polarization losses (according to eq. (1)). In order to do that, the user must set the value of the current density and the utilization factor as input values: indeed, the average composition of the streams flowing through the anode and cathode is used to compute Nernst potential and voltage losses, and depends on the inlet compositions and on the values of $U_{CO2}/U_{O2}/U_F$.

In the stand-alone application (i.e. without CO_2 capture), the MCFC cathode is fed with air and recycled anode exhausts, in order to provide both the O_2 and the CO_2 required for sustaining electrochemical reactions (see Fig. 2, Case A). Since targeting a complete fuel conversion (i.e., 100% fuel utilization factor) would lead to excessive concentration losses and shorter fuel cell life, the MCFC anode is fed with excess fuel (the typical fuel utilization factor U_F is 70–80%) and the unconverted syngas (made by H_2O, CO and H_2) is mixed with air and oxidized in a catalytic combustor before being fed to the cathode. In this way, the thermal power generated by the syngas combustion brings the temperature of cathode stream up to the MCFC working condition. On the other side of the fuel cell, cathode exhausts are cooled by preheating NG and water fed to the anode.

Since all the anode effluents are recycled back to the MCFC cathode, the inlet CO_2 partial pressure at the cathode side is quite high ($p_{CO2ct} \sim$ 15–20%), and allows the fuel cell to work with high voltage (see eq. (2)) and high electric efficiency, owing also to the low CO_2 utilization factor. Indeed, in this condition the MCFC can reach high voltages (e.g., around 0.8 V) even in case of high current densities ($IC = 1500$–1600 A m^{-2}).

When the MCFC is operated in a carbon capture configuration (Fig. 2, case B), the fuel cell operates as an active CO_2 concentrator, and the CO_2 partial pressure at the cathode inlet is usually lower, because it is defined by the composition of combustion effluents coming from the source combustion process (e.g., in the present case NGCC exhausts @4%CO_2). In addition, the likely high CO_2 utilization factor (required to

Table 1
Fuel cell operating parameters [12].

Fuel utilization factor (single pass)	75%
Steam to carbon ratio (S/C)	2
Current density	1500 A m^{-2}
CO_2 mol fraction at cathode outlet (X CO_2)	1%
Inlet temperature (reforming layer)	450 °C
Inlet temperature (anode and cathode)	580 °C
Pressure losses on anode/cathode	3/2 kPa
Heat losses (% input thermal power)	1%
DC/AC converter efficiency	94%

match the targeted CO_2 capture levels of 80–90%) brings the average CO_2 concentration across the cathode down to low values. For this reason, if the fuel cell is operated with the same current density of the standalone capture configuration (e.g., $IC = 1500$ Am^{-2}), the voltage will be lower than that observed in the standalone case (e.g., 0.7 V instead of 0.8 V) [12].

Fig. 3-A illustrates the resulting MCFC voltage and its efficiency as a function of CO_2 concentration at the cathode inlet. Fig. 3-B shows the effect of current density and fuel utilization factor on the MCFC voltage, for a case representative of the MCFC integration to NGCCs ($X_{CO2} = 4\%$ at the cathode inlet). Since the ohmic polarization is directly proportional to the value of current density, the MCFC voltage shows a linear decrease as current density (IC) increases. Likewise, a minor voltage loss is observed also as the fuel utilization factor (U_F) increases, because of the progressively lower average H_2 partial pressure across the anode.

It is important to highlight that the U_F values represented on the x-axis of Fig. 3-B are related to a single passage of the fuel through the MCFC. As explained in the next section and already illustrated in Fig. 2, one advantage of the carbon capture configuration is the possibility of recycling the unconverted syngas from the anode outlet to the anode inlet, increasing the overall fuel utilization (up to 100%) and the electric efficiency of the capture system. This efficient configuration is prompted by the need of separating the unconverted fuel from the CO_2-rich anode exhausts, with the aim of matching the specifications of the CO_2 stream sent to transport and storage facilities.

The MCFC operating conditions assumed for the NGCC + MCFC configurations here assessed are listed in Table 1, reflecting the current state of technology developed by FCE. The selected current density (IC = 1500 A m^{-2}, Table 1) is a trade-off between the need to maximize the power density and minimize the MCFC active area and the related investment cost. The increase of the current density raises the ohmic overpotential, which causes a decrease of the fuel cell voltage and a consequent efficiency penalty on the MCFC based capture system. As illustrated in Fig. 3-B, if the current density is increased from 1100 A m^{-2} to 1500 A m^{-2} the higher ohmic resistance of the fuel cell decreases its voltage from the value of 0.75 V down to 0.7 V. Hence, the voltage percentage decrease is less significant than the corresponding current density increase: for this reason, a higher current density means also a higher power density ($P_{spec} = V^*IC = 1050$ W m^{-2}) and a lower investment cost. Nevertheless, the high over-potential and the related waste heat caused by high current density and high utilization factors could affect the integrity of the electrolyte and the electrodes, whose durability should be experimentally demonstrated in dedicated long period test, representative of CCS working conditions.

The fuel utilization factor related to a single pass of the MCFC (U_F) is assumed equal to 75%, whereas the input value for CO_2 utilization factor (U_{CO2}) results from another assumption related to the MCFC operation limits. Indeed, U_{CO2} is calculated to have a CO_2 concentration of 1% at cathode outlet, in order to avoid large concentration overpotential inside the MCFC. In this first case, since the MCFC cathode receives the CO_2 in the NGCC exhaust (@3.98% CO_2, 12.39% O_2), the resulting CO_2 utilization is roughly $U_{CO2} = 76\%$. In the final sensitivity analysis presented in section 7, the minimum CO_2 concentration is varied between 0.5 and 2%, obtaining U_{CO2} values between 50 and 90%.

The value of the MCFC voltage combined with the reactants' mass flow rates and their inlet and outlet compositions (the latter determined by the utilization factors) is used to close the energy balance of the fuel cell. In particular, the temperature increase across the MCFC layers can be calculated by assuming that the anode and cathode streams leave the fuel cell at the same temperature. Despite the significant voltage losses associated to the combination of (i) high current density and (ii) high CO_2 utilization factors, heat management does not appear as a critical issue for the stack operation: neither in the integrated, nor in the non-integrated cases the temperature increase exceeds the safety values commonly considered for the operation (e.g. $\Delta T < 70$ °C), owing to the large thermal capacity of the GT effluents fed to the MCFC cathode.

3. Proposed NGCC-MCFC schemes

Two MCFC and NGCC applications have been selected and studied in this work: the schemes of both the integrated and non-integrated ("fully-retrofitable") layouts are illustrated, respectively, in Fig. 4 and Fig. 5. The first integrated option already discussed in Ref. [12] is one of the most efficient CCS power plant concepts, because of the combination of high MCFC electric efficiency and favourable heat integration: the MCFC is placed between the GT and the HRSG and separates the CO_2 from the high temperature GT exhausts (#5). This "intermediate" position of the fuel cell modules reduces the energy penalty associated with the CO_2 capture process, because the temperature of cathode inlet stream (GT exhausts @608 °C) matches well with the MCFC's working temperature (580 °C), and owing to the absence of cathode reactants preheating section, the waste heat released by the MCFC is exploited in the Heat Recovery Steam Cycle (HRSC) for generating additional steam, improving the power output of the bottoming Rankine cycle. After being purified from most of the CO_2 inside the MCFC, cathode exhausts (#6) are fed to the HRSC still at high temperature (650 °C). On the other side of the MCFC, anode reactants (NG, H_2O) are first preheated to 300 °C by exploiting the high pressure water produced in the HRSG, then sent to the desulphurization unit. Finally, this stream (#9) is directly mixed with superheated steam extracted from the HRSG, with the aim of providing the steam to carbon ratio and the inlet temperature required by the pre-reformer layer integrated to the MCFC unit (S/C = 2, T = 450 °C). Anode exhausts are mainly composed by CO_2, H_2O and unconverted syngas (CO and H_2 residues).

The stream leaving the anode (#11), which contains the unconverted H_2/CO stream and the CO_2-rich flow, first produces steam in separate section of the HRSG (in order to avoid the self-defeating dilution with cathode reactants) and then enters the GPU section (#12), where CO_2 is separated from the unconverted fuel (#13) via the double-flash cryogenic gas purification unit described in section 4, designed to match the CO_2 purity specifications for transport and storage (#14). In order to maximize the overall fuel utilization and the efficiency of the fuel cell section, the unconverted fuel recovered by the cryogenic section is recycled back to the fuel cell anode. Before being introduced to the MCFC, the unconverted fuel is preheated up to 300 °C together with natural gas, sent to the zinc-oxide sulfur removal unit [31] and then heated up to the anode inlet temperature (450 °C) by direct mixing with superheated steam (#15, 565 °C) extracted from the LP section of the steam cycle. As a result, the anode is fed with a mixture (#10) of natural gas, recovered syngas and steam, whose mass flow rate is calculated to ensure a S/C equal to 2.

The configuration of the heat exchanger network has been optimized targeting the maximum heat recovery (i.e., maximum generation of steam to be expanded in the steam turbine) and taking into account the metal dusting issue [32] which may affect the anode side heat exchangers. Since the anode inlet and outlet streams contain CO and H_2 with a carbon activity greater than 1 in the temperature range 450–800 °C (in absence of H_2S), severe carburization may occur causing the progressive disintegration of the heat exchanger metal walls. To prevent this damage, the metal temperature of coolers is kept below

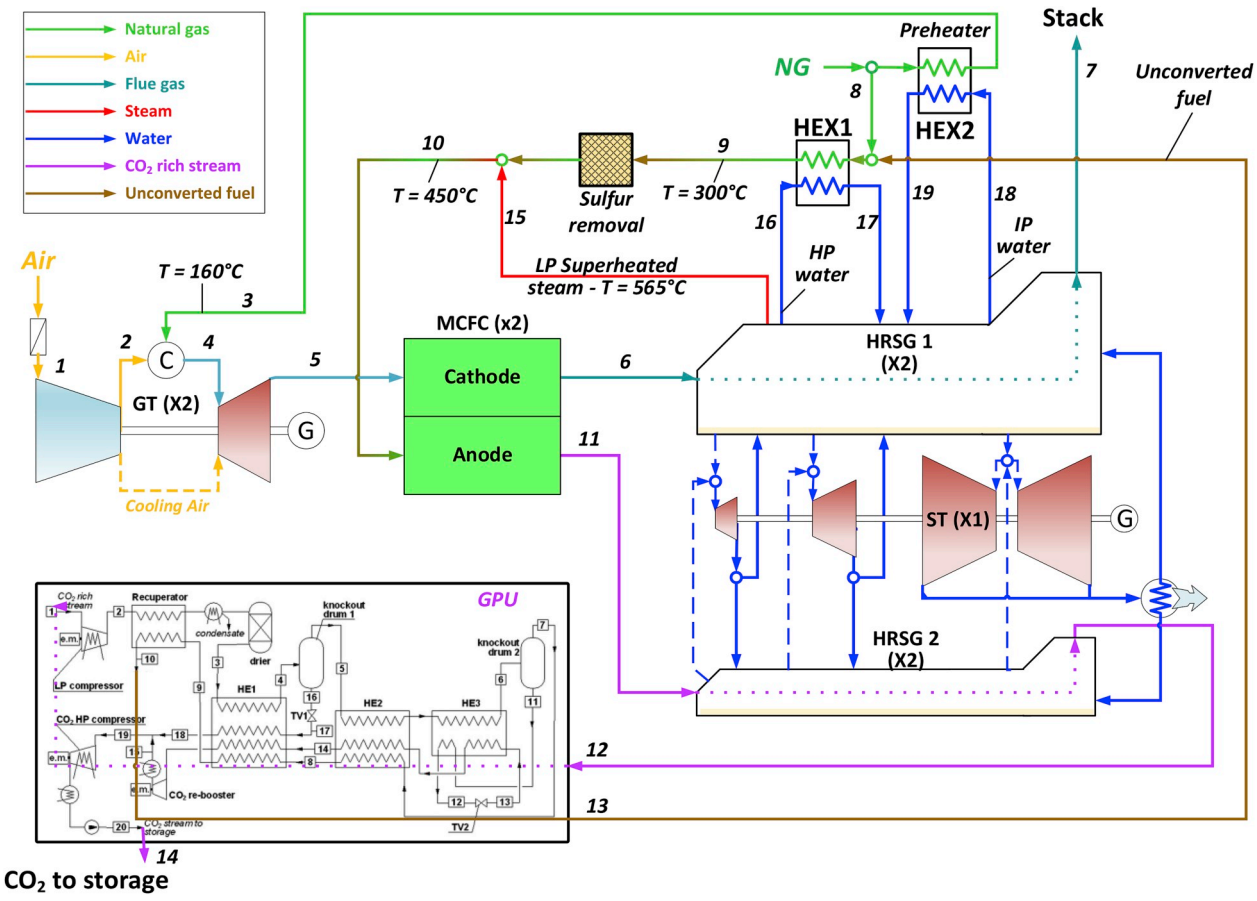

Fig. 4. Layout of the integrated MCFC + NGCC option (the actual GPU scheme is reported in Fig. 6).

450 °C by evaporating steam or preheating liquid water (whose high heat transfer coefficient allows keeping the tube temperature close to the steam evaporation temperature) while the anode fuel is heated up from 300 °C to 450 °C by mixing superheated steam.

In the non-integrated option (Fig. 5), the MCFC is placed downstream the HRSC, in order to avoid the need of any modification to the NGCC: this solution fits perfectly also with the strategy of retrofitting existing NGCCs, with minimal variation on the operation of the baseline

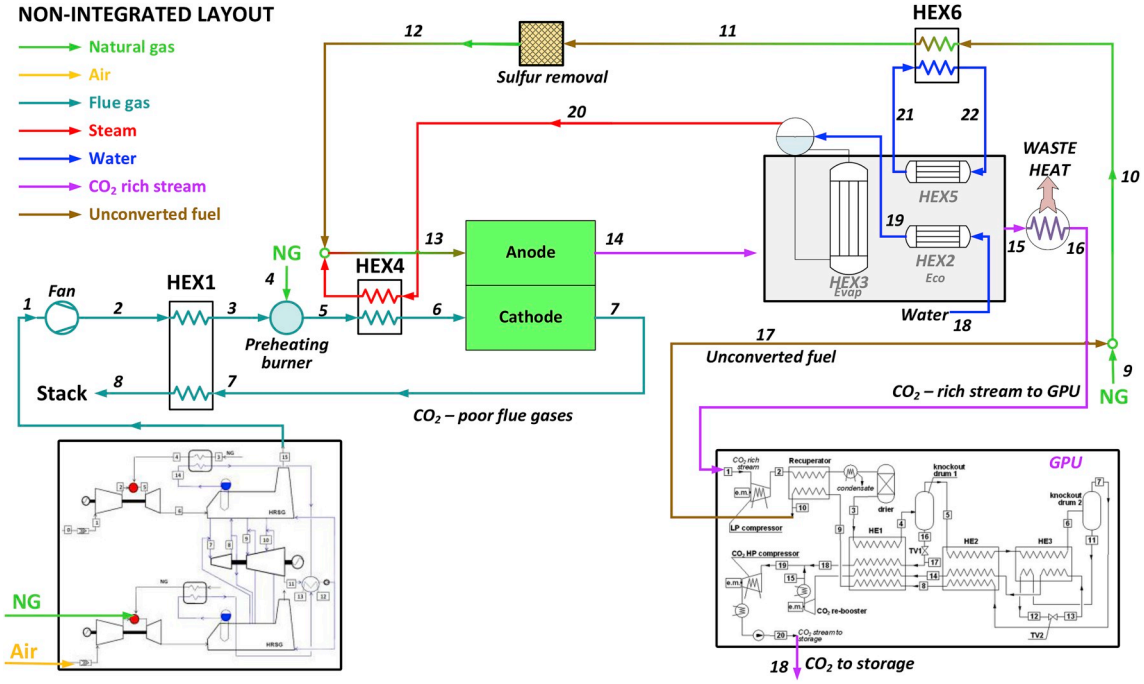

Fig. 5. Layout of the non-integrated MCFC + NGCC option (the actual GPU scheme is reported in Fig. 6).

power plant. The non-integrated option is less invasive but also inherently less efficient than the integrated one, because the fuel fed to the MCFC is converted to electricity with a lower efficiency, which results from the power production of the MCFC modules only. In this "bolt-on" configuration, the fuel cell is not followed by a bottoming cycle: as illustrated in Fig. 5, all the heat transfer surfaces needed to cool down MCFC effluents are not exploited for generating steam for power production but only used to preheat the MCFC inlet streams. Hence, as confirmed in the results section, the relative simplicity of the non-integrated scheme is partly counterbalanced by a more complicated heat exchanger network, which contributes to increasing capital cost of the CO_2 capture section.

The additional cathode stream preheater (stream #2, HEX1), required to raise the stream temperature from the HRSC outlet (87 °C) up to the MCFC level (i.e., 580 °C at the inlet of the cathode), is identified as the most critical component of the heat transfer network, due to the large heat transfer area resulting from the high mass flow rate of the cold/hot streams (#2/#7) and the low LMTD (around 70 °C). On the other hand, the installation of HEX1 is essential for achieving reasonable performance in the non-integrated plant, because the sole use of an auxiliary burner fed by NG (#5) would penalize dramatically the performances of the power plant. Due to the large mass flow rate of the cathode stream (#2, around 1350 kg s^{-1}), if the full preheating process (from the stack temperature to the MCFC temperature) was carried out by the preheating burner, the efficiency drop would exceed 20% points. Naturally, this efficiency penalty could be partly limited by raising steam in a dedicated HRSC fed by the hot cathode exhausts, but this choice would require additional capital cost and would put the layout far from the "non-integrated" concept. Hence, cathode gas is first preheated up to an intermediate temperature by a rotary-type regenerative heat exchanger (with MCFC cathode exhausts on the hot side, #7-8) and then heated up to the target MCFC working temperature by the auxiliary NG burner, accepting the efficiency penalty associated with the use of NG for low temperature preheating. Since the share between the thermal power exchanged by regenerative heat exchanger HEX1 and by the auxiliary burner has a significant influence on both power plant capital costs and its electric efficiency, the intermediate (#4) temperature has been optimized by minimizing the cost of CO_2 avoided, obtaining a value of 530 °C.

Four parallel Ljungstrom type heat exchangers have been designed for sustaining the preheating duty of the cathode stream (around 670 MWt), using the ε-NTU iterative method described in Ref. [33].

The constraints associated to the metal dusting issue preclude the possibility of exploiting the hot anode exhaust (#14) to complete the preheating process of the cathode stream. Thus, HEX2, HEX3 and HEX5 produce the steam required by the fuel cell (#18-19-20, HEX2/HEX3) and the hot water (#21-22, @175 bar/350 °C) used for the indirect NG preheating (HEX5): due to the high heat transfer coefficient of the cold side, the wall temperature in these heat exchangers is safely below the critical level of metal dusting. Finally, the shell-and-tube NG preheater (HEX6) uses liquid water produced by HEX5 as hot medium (#21-22), whereas steam superheater tube banks are used for producing the steam sent to the MCFC anode (#13, HEX 4). For this second option, the cryogenic purification unit features the same design as the integrated scheme. Almost all the unconverted syngas released with the CO_2-rich effluents from the anode outlet is recycled to the anode inlet, approaching the complete fuel utilization.

All the power plants simulations have been carried out using GS software [30] and the commercial softwares Aspen Plus [34] and Thermoflex [35]. The heat and mass balances of the NGCC and MCFC sections have been calculated with GS, while the GPU has been modelled and simulated in Aspen Plus (hence GS and Aspen Plus are integrated via the anode exhaust and unconverted recycle streams).

On the other hand, Thermoflex has been used to estimate design, sizing and cost of the quench boiler of the integrated layout (two parallel HRSGs cooling the anode exhaust stream as in Fig. 4), as well as of the quench boiler, HEX4 and HEX5 of the non-integrated option (Fig. 5).

The NGCC considered as a reference case is presented in the CCS EBTF report [5], and already described in Ref. [12]. The power plant without CCS achieves $\eta_{el,LHV} = 58.3\%$ with a P_{el} of 829.9 MW_{el} and specific emissions of 351.8 g_{CO2} kWh_{el}^{-1}, whereas the same NGCC with MEA-based post-combustion CCS features $\eta_{el,LHV} = 49.9\%$ with a CCR of 90%. The key assumptions used for the power plant simulations are reported in Table 2.

4. Gas processing unit

As highlighted in section 3, the lower the fuel utilization factor U_F,

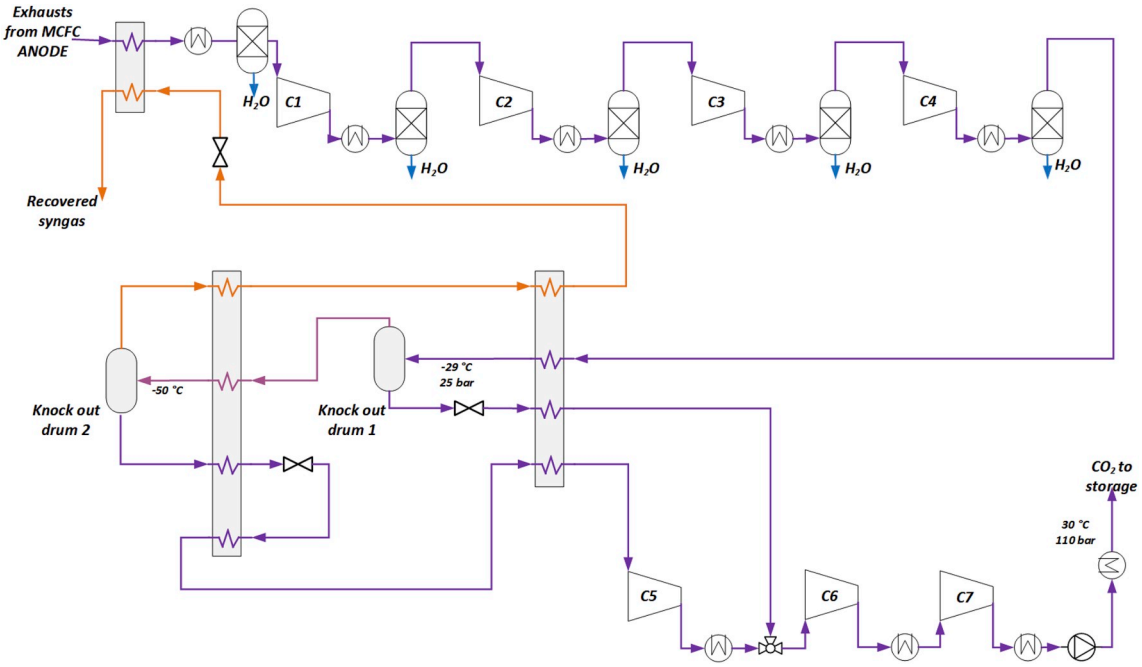

Fig. 6. Layout of the gas processing unit.

Table 2
Key assumptions for evaluation of baseline and carbon capture layouts.

Ambient conditions	15 °C/1.013 bar/60% humidity
Natural gas conditions	10 °C/70 bar
Gas turbine – two F-class machines	
Pressure ratio, β	18.1
Turbine inlet temperature, TIT, °C	1360
Gas turbine efficiency, %LHV	38.25
Heat recovery steam cycle – 3 pressure levels, bar	130/35/4
Superheat temperature, °C	565
Condensing pressure, bar	0.048
Cooling water temperature, °C	18
Temperature at outlet of coolers, °C	28
Electric consumption of auxiliaries for cooling, % of the heat rejected	2
Condensing temperature of refrigerators (where required), °C	32
Polytropic efficiency of flue gas compressors, %	90
Polytropic efficiency of flue gas expanders, %	90
Polytropic efficiency of vacuum pumps, %	85
Polytropic efficiency of CO_2 compressors, %	85
Polytropic efficiency of air blowers, %	85
Hydraulic efficiency of CO_2 pumps, %	75
Electric-mechanical efficiency of motor-drivers, %	95
Minimum temperature difference gas-gas heat exchangers, °C	25
Minimum temperature liquid-gas heat exchangers, °C	10
Relative pressure drop of heat exchangers - gas side, %	2
Relative pressure drop of heat exchangers - liquid side, bar	0.4
Pressure drops in the HRSG, mbar	20

the more stable to operate and more durable the MCFC is, thanks to a reduced concentration overpotential. Even though it is CO_2-rich (the CO_2 content is 80%mol for the non-integrated case and 83%mol for the integrated case), the anode stream discharged by the MCFC is not suitable for final geological storage or Enhanced Oil Recovery (EOR) applications. Therefore, the anode stream needs to be purified in order to increase the CO_2 concentration by removing residual inert species (H_2O and N_2) and by recovering the unconverted fuel (CO and H_2) [16]. As a consequence, the CCS plant must include a CO_2 compression and purification unit, designed to achieve the following goals:

- to match the CO_2 quality standards typically envisaged for long range pipeline transport and EOR (reported in Table 3);
- to recover as much as possible the valuable fuel species (CO and H_2) which leave the MCFC as unconverted stream. Indeed, the anode stream still contains a significant amount of primary energy (around 30% of the MCFC fuel input leaves the anode unreacted), which must be recovered and recycled back to the fuel cell, in order to maximize the overall fuel utilization factor and the plant efficiency.

Owing to the high CO_2 concentration in the anode stream, the required CO_2 purification can be efficiently achieved by the cryogenic, auto-refrigerated, double-stage flash separation process represented in Fig. 6.

In particular, this system exploits a multi-stage compression process [16], in which pressurized CO_2 is partly condensed with auto-refrigeration and separated from condensable gases at low temperature via a two-stage phase-change process. The auto-refrigeration effect is achieved by using the flashed CO_2-rich liquid streams as cooling sources. The GPU produces dense-phase CO_2 at 110 bar, whereas the recovered gaseous stream (containing mostly H_2 and CO) is preheated and recycled back to the MCFC section. The main advantages of this GPU system are the absence of additional chemical or physical solvents and relatively low energy consumption (531 MJ t_{CO2}^{-1} for the integrated scheme and 579 MJ t_{CO2}^{-1} for the non-integrated layout) compared to alternative solutions. The assessed system is able to bring the CO_2-rich stream up to a final purity of 98.9%mol, with a CO_2 recovery efficiency

Table 3
CO_2 specifications for the EOR application envisaged.

Parameter	Value
Temperature, °C	30
Pressure, bar	110
CO_2, %mol	>97
H_2O, ppm_v	<50
N_2 and other non-condensables, %mol	<3
O_2, ppm_v	<75

of 90%: the rest of the treated CO_2 is removed from the GPU as gaseous phase (orange stream in Fig. 6) together with most of the unreacted syngas and finally recycled back to the MCFC anode.

5. Methodology and main assumptions for the economic evaluation

The economic analysis is based on the generic bottom-up approach conceptually illustrated in Fig. 7, which reports also the most relevant economic and financial assumptions used to estimate the cost of electricity (COE) and the cost of CO_2 avoided (CCA). The first operation involves the evaluation of the Total Plant Cost (TPC), associated to the installation of the NGCC + MCFC system. The TPC is calculated by dividing the power plant and the CO_2 capture system into relevant subsections/components, developing an adequate cost correlation for each of them and finally adding the installation, contingencies and indirect costs. In particular, the procedure requires the calculation of several intermediate cost values:

- Total Equipment Cost (TEC, Table 4) which results from the sum of the equipment costs of all the plant components. Each single cost has been obtained by using a typical power-law function obtained from technical reports or simulation codes (i.e., Aspen plus [34], Thermoflex [35]), that associate the equipment cost to the most representative size parameter of the specific component. As an example, the cost of the Ljungstrom wheels for the non-integrated option has been estimated using the relevant correlation described in Ref. [36], which takes into account the effect of gas leakages (evaluated during the Ljungstrom design) and the effect of high temperature sections, resulting in a total equipment cost of around 30 M$. As represented in Fig. 5, the units HEX2, HEX3, HEX5 and the waste heat recovery boiler have been sized and costed as a unique assembly, using HRSG cost functions, despite the less challenging steam parameters and small size. The reference equipment cost for the MCFC stack (a constant, specific cost of 465 $ m^{-2}, based on cost information already exploited in Ref. [27]) is one of the most uncertain assumptions, because it is based on future mass-production of the stack components (i.e., hundreds of MW per year).

Since, there is not yet a mature MCFC market, the cost of MCFC modules is very difficult to predict. However, the cost assumed here is in line with the ranges reported by manufacturers, which span from 2000 $ kW_{el}^{-1} for a 5 MW_{el} annual production to 1250 $ kW_{el}^{-1} for a 50 MW_{el} yearly demand [37].

- Total Direct Plant Cost (TDPC), which is obtained by adding to the TEC all the costs related to equipment installation;
- Engineering, Procurement and Construction (EPC) cost, calculated by adding to the TDPC the indirect cost related to engineering, buildings and site improvement;
- Total Plant Cost (TPC), which results from the sum of the EPC cost and the cost associated to all the project planning and contingencies.

As reported in Fig. 7, the installation, indirect and project cost contingency are expressed as a fraction of TEC, TDPC and EPC values:

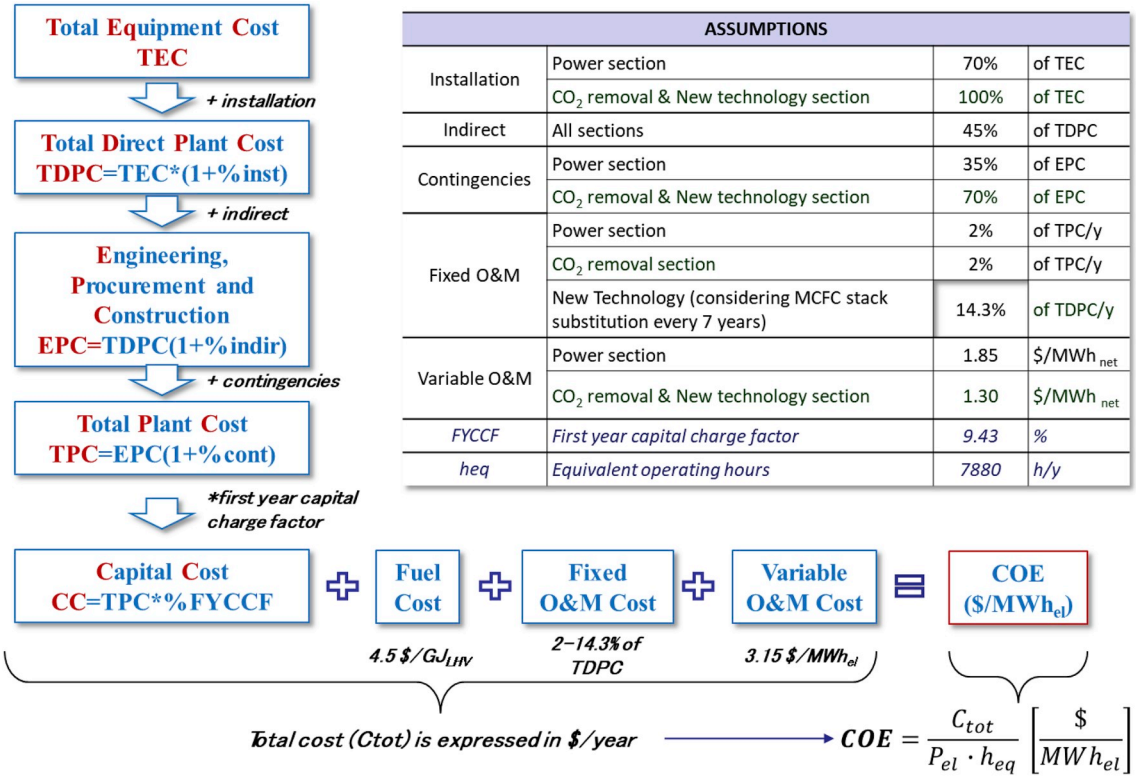

ASSUMPTIONS			
Installation	Power section	70%	of TEC
	CO_2 removal & New technology section	100%	of TEC
Indirect	All sections	45%	of TDPC
Contingencies	Power section	35%	of EPC
	CO_2 removal & New technology section	70%	of EPC
Fixed O&M	Power section	2%	of TPC/y
	CO_2 removal section	2%	of TPC/y
	New Technology (considering MCFC stack substitution every 7 years)	14.3%	of TDPC/y
Variable O&M	Power section	1.85	$/MWh$_{net}$
	CO_2 removal & New technology section	1.30	$/MWh$_{net}$
FYCCF	*First year capital charge factor*	*9.43*	*%*
heq	*Equivalent operating hours*	*7880*	*h/y*

Fig. 7. Schematic sequence of cost estimation and assumptions for the economic model.

hence, the total plant cost is obtained by multiplying the TEC by a series of incremental factors (%inst, %indir, %cont in Fig. 7). Since the readiness level of the specific technology influences the relative extent of installation, engineering and contingency contributions, the values assumed for these percentage factors are different for each one of the plant sections. Indeed, if some components can be reasonably classified as mature technologies (e.g., GT), other components/subsections (CCS equipment) are still characterized by a lower level of confidence from both the engineering and economic perspectives. As an example, the contingencies associated to the capture section are much higher than the value related to the power section (70% vs 35%), because the carbon capture section features higher project uncertainties, mainly related to the lower technological maturity (i.e., TRL) and more limited industrial experience of some key pieces of equipment or plant sections (e.g., MCFC, cryogenic unit, etc.) compared to conventional ones.

Once the TPC is obtained, the economic analysis involves the calculation of the First Year Cost of Electricity (COE), obtained by combining the total capital cost with the cost of fuel, consumables and O&M. These cost values are calculated according to the technical and financial assumptions of Fig. 7 and to the CCP methodology described in Ref. [38] (Chapter 4). The analysis is then concluded by calculating the cost of CO_2 avoided (CCA – eq. (4)), which is generally recognized as the most significant benchmark index for the techno-economic evaluation of CCS systems. The CCA [$\$\ t_{CO2}^{-1}$] can be calculated as the ratio between the marginal cost of the electricity for the MCFC + NGCC power plant and the avoided specific CO_2 emission:

$$CCA = \frac{(COE)_{CCS} - (COE)_{REF}}{(e_{CO2})_{REF} - (e_{CO2})_{CCS}} \quad \left[\frac{\$}{t_{CO2\ avoided}}\right] \tag{4}$$

Table 4
Equipment costs for the integrated/non-integrated layouts (M$2014).

Total Equipment Cost	Integrated	Non-integrated
GT, M$	134	134
Steam Cycle, M$	136	130
Total Equipment Cost of power section, M$	*269*	*264*
Equipment cost of GPU, M$	44	46
MCFC + BOP, M$	99	115
Flue gas blower, M$	2	3
Fuel heaters, M$	7	0.3
Quench boilers, M$	13	11
Cathode stream heaters, M$	-	31
Total Equipment Cost of CO_2 removal section, M$	*164*	*159*

6. Results and costs for the proposed integrated and non integrated schemes

Simulation and calculated results for the integrated and non-integrated layouts are reported in Table 5, whereas the properties of the main streams (numbered in Figs. 4 and 5) are reported in Appendix A. Simulation results confirm the good performances of the integrated system, which can avoid nearly 80% of CO_2 emissions with a limited energy penalty: if compared with the baseline NGCC, the net electric efficiency of the MCFC + NGCC power plant is reduced by less than 1%. Compared with the reference NGCC without capture, the HRSC power of the integrated case increases by 7% owing to the rise of flue gas temperature (the MCFC increases the flue gas temperature by 72 °C) and its mass flow rate, which is increased by the contribution of the NG and water feeding the MCFC anode. Both CO_2 and O_2 utilization factors result from the assumption on the minimum concentration of CO_2 (U_{CO2} and U_{O2} are respectively 75.9% and 12.1%), which is the limiting specie for the electrochemical reaction on the cathode side. Naturally, all the CO_2 generated by NG oxidation in the anode side is directly concentrated in the anode exhaust gas, and makes the CO_2 capture rate (79.7%) higher than the CO_2 utilization factor. Finally, the limited efficiency penalty and the significant carbon capture rate of the integrated solution are reflected in the value of the SPECCA, which approaches 0 MJ kg_{CO2}^{-1}, as already observed in previous studies on this CO_2 capture configuration [17].

Table 5
General performance and costs of the NGCC + MCFC integrated and non-integrated layouts.

Power balance - NGCC + MCFC	Reference case	Integrated	Non-Integrated
GT - Net electric power, MW_{el}	544.2	542.9	544.2
Steam Cycle - Net electric power, MW_{el}	285.7	305.57	289.9
MCFC - Net electric power (w/o aux), MW_{el}	-	179.08	192.6
Auxiliaries (fan), MW_{el}	-	2.35	8.74
GPU consumption, MW_{el}	-	41.80	48.82
Fuel input, MW_{LHV}	1422.6	1709.4	1839.5
Overall net electric power, MW_{el}	829.9	983.4	969.1
Net electric efficiency	58.3%	57.53%	52.68%
CO_2 Balance			
CO_2 from NGCC, kg s^{-1}	81.63	81.63	81.63
CO_2 from MCFC, kg s^{-1}	-	16.4	23.76
Carbon capture rate	-	79.75%	81.1%
CO_2 specific emissions, g kWh_{el}^{-1}	351.8	72.18	73.82
CO_2 avoided, g kWh_{el}^{-1}	-	279.62	277.98
CO_2 avoidance rate	-	79.48%	79.0%
SPECCA, MJ kg_{CO2}^{-1}	-	0.310	2.382
Economics			
COE, $ MWh_{el}^{-1}	45.0	58.80	66.08
Cost of CO_2 avoided, $ t_{CO2}^{-1}	-	49.37	75.85

The proposed layout appears very promising also from the economic perspective, owing to the excellent performances that limit the cost of CO_2 avoided to 50 $ t_{CO2}^{-1}.

In the non-integrated scheme, the electric power produced by the MCFC section increases up to 193 MW_{el}, (+7.5% with respect to the integrated case). The increase of MCFC power output depends on the fuel burned in the combustor to raise the cathode stream up to the MCFC working temperature. The preheating combustion generates a supplementary stream of CO_2 which has to be separated in the cathode side of the fuel cell, increasing the total current generated by the electrochemical reaction and the power output produced by the MCFC modules. As a result, the integrated layout elevates the CO_2 capture rate up to 81.1%, owing to the larger size of the MCFC section and to the consequent larger amount of CO_2 generated in the anode, which is fully captured in the MCFC-GPU loop. On the other hand, the CO_2 avoided decreases to 79% because the non-integrated system features a lower electric efficiency (−4.8% with respect to the integrated solution) and, as a consequence, higher specific CO_2 emissions. Nevertheless, the SPECCA index is low also for the non-integrated option, being more promising than the benchmark value representative of chemical absorption processes with amine-based solvents (SPECCA = 2.5–3.5 MJ kg_{CO2}^{-1}). The economic analysis shows that the cost of CO_2 avoided of the non-integrated scheme is about 50% higher than the integrated case; the primary reason is the lower electric efficiency of this solution, which is mainly penalized by the use of NG for low temperature preheating and the strategic choice of avoiding any heat integration with the existing NGCC. In addition, the CCA is penalized by the investment cost of the additional pre-heater of the cathode stream.

Considering a conventional MCFC module made up of 8 parallel stacks, each composed of 400 cells with an active area of 0.7 m^2 for each cell, the resulting MCFC-based capture section will include roughly 75 and 80 modules respectively for the integrated and non-integrated cases. Therefore, besides the significant footprint of the MCFC equipment, which is one of the well known drawbacks of fuel cells, its installation will require a first of a kind design (because no multi-MW plants exist for CCS with fuel cells) of the proper piping network, capable of splitting the large GT flow rates into a large number of parallel streams to be fed to the cathode sections of the MCFC modules.

7. Sensitivity analysis on CO_2 utilization factor

This section presents the sensitivity analysis on the CO_2 utilization factor for both the integrated and non-integrated solution which has been carried out to explore its effect on performance and costs. This analysis implies that the fuel cell can work in safe and stable conditions even if the minimum CO_2 concentration at cathode outlet is pushed below the recommended value of 1%: despite this operating condition has been experimentally proven (down to a CO_2 concentration of 0.5%), this assumption should be further validated by pursuing long-term operational tests. The sensitivity analysis considers three levels of CO_2 concentration at cathode outlet: 2%, 1% (reference value) and 0.5%. The resulting CO_2 utilization factor is reported in the third line of Table 6 and range between 51% and 89%.

The results reported in Table 6 show the following effects:

- in both the integrated and non-integrated options, an increase of U_{CO2} leads to a decrease of MCFC voltage and a consequent efficiency penalty. This is caused by the lower average CO_2 concentration in the cathode stream, which decreases the value of Nernst potential (E_{Nernst}, eq. (2)) and increases the activation losses (ΔV_{act});
- the overall electric power increases with U_{CO2}, because the total current generated by the fuel cell modules is proportional to the flow rate of CO_2 molecules migrated from the cathode to the anode. This effect overcomes the decrease of MCFC voltage discussed in the

Table 6
Results of the sensitivity analysis on CO_2 utilization factor, for the integrated and non-integrated MCFC + NGCC schemes.

Power balance - NGCC + MCFC	Integrated			Non-integrated		
CO_2 concentration at cathode outlet	2%	1%	0.5%	2%	1%	0.5%
CO_2 utilization factor, U_{CO2}	51%	75.9%	88%	54%	77.4%	88.8%
GT - Net electric power, MW_{el}	542.9	542.9	542.9	544.2	544.2	544.2
HRSG - Net electric power, MW_{el}	300.48	305.57	308.27	288.1	289.9	292.1
MCFC - Net electric power, MW_{el}	121.94	179.08	206.26	134.9	192.6	219.3
Auxiliaries, MW_{el}	2.45	2.35	2.33	8.835	8.745	8.722
GPU consumption, MW_{el}	28.07	41.80	48.50	34.02	48.82	56.30
Fuel input, MW_{LHV}	1615.5	1709.4	1755.3	1736.0	1839.5	1886.8
Overall net electric power, MW_{el}	934.8	983.4	1006.6	924.4	969.1	990.5
Net electric efficiency	57.86%	57.53%	57.35%	53.25%	52.68%	52.5%
CO_2 Balance						
CO_2 from NGCC, kg s^{-1}	81.63	81.63	81.63	81.63	81.63	81.63
CO_2 from MCFC section, kg s^{-1}	11	16.4	19.1	17.85	23.76	26.45
Carbon capture efficiency	56.54%	79.75%	90.24%	59.5%	81.1%	90.6%
CO_2 specific emissions, g kWh_{el}^{-1}	154.2	72.18	34.94	157.06	73.82	36.93
CO_2 avoided	56.15%	79.48%	90.07%	55.4%	79.0%	89.5%
SPECCA, MJ kg_{CO2}^{-1}	0.256	0.310	0.335	3.029	2.382	2.18
Economics						
COE, $ MWh^{-1}	55.56	58.80	60.27	63.20	66.08	67.73
Cost of CO_2 avoided, $ t_{CO2}^{-1}	53.43	49.37	48.18	93.48	75.85	72.19

Table 7
Techno-economic comparison between MEA and MCFC cases – summary table.

	NGCC + MEA	NGCC + Integrated MCFC	NGCC + Non-integrated MCFC
SPECCA, $MJ_{LHV}\ kg_{CO2}^{-1}$	3.34	0.31	2.38
CCR, %	90.5	79.7	81.1
Specific energy penalty, $MJ_{el}\ kg_{CO2}^{-1}$	1.63	0.18	1.23
Specific cost of the CO_2 capture unit, $ kW_{el}^{-1}	977	820	1043
Specific cost of the overall plant, $ kW_{el}^{-1}	2181	1731	1950
COE, $ MWh_{el}^{-1}	68.6	58.8	66.1
CCA, $ t_{CO2}^{-1}	74.7	49.4	75.9

previous point. In addition, the double effect related to (i) the larger amount of NG and water fed to the MCFC and (ii) the larger waste heat produced by the higher voltage losses determines also an indirect increase of the HRSC power output;

- the CO_2 capture efficiency improves with U_{CO2} because of the direct effect related to the larger amount of CO_2 separated from the cathode stream and because the fraction of CO_2 generated from the fuel cell itself (generated by NG converted into the anode and then fully captured) increases with the MCFC power.

Interestingly, the resulting SPECCA values delineate opposite trends in the integrated and non-integrated options. Indeed, the first three values of the integrated configuration are almost constant and unrelated to the value of U_{CO2}: the slight decrease of SPECCA (from 0.335 to 0.256 MJ kg_{CO2}^{-1}) depends on the higher voltage (meaning lower concentration polarization) promoted by the higher CO_2 partial pressure at the cathode side of the fuel cell. Vice versa, the non-integrated option shows a positive effect of high carbon capture designs (the higher the CO_2 utilization factor, the lower the SPECCA). The main reason of this behaviour can be found in the energy balance of the preheating section, where NG combustion is exploited to complete the cathode stream preheating process. Indeed, this fraction of primary energy introduced in the CO_2 capture section does not depend on the extent of the CO_2 capture rate (which defines the size of the fuel cell stack and its power output) but only on mass flow rate of cathode exhausts. In other words, it can be easily noticed that:

- the fraction of NG sent to the MCFC anode is proportional to the CO_2 permeated from the cathode to the anode of the fuel cell; the higher the CO_2 utilization, the higher the NG utilization.
- the fraction of NG burned in the preheating section is roughly constant and does not depend on CO_2 utilization, because all the NGCC exhausts must be heated up to the MCFC working temperature even in case of poor CO_2 separation.

As a result, in the cases with low CO_2 capture (low U_{CO2}) the constant amount of primary energy introduced for preheating all the gas mass flow rate (meaning higher *specific* primary energy for capturing 1 molecule of CO_2) is reflected by the penalizing trend of the SPECCA, which increases accordingly to this effect. This occurs also in the cost of CO_2 avoided, whose increase is much higher in the non-integrated case (+30% going from the low capture case to the high capture case) than in the integrated solution (+10% going from the low capture case to the high capture case). As a conclusion, high carbon capture configurations are essential for featuring high performances especially in the non-integrated case, where a fraction of the primary energy introduced in the capture system doesn't depend on the CO_2 capture rate.

8. Discussion and conclusions

The performance found in this work should be compared with those of a benchmark CO_2 capture process in order to assess the potential of the proposed schemes. As benchmark CO_2 capture process we consider the post-combustion MEA scrubbing system assessed in the EBTF report [39]. Indeed it is one of the most well-proven processes for CO_2 capture and its technological readiness is demonstrated by the presence of several pilot/demo plants in operation [40]. The comparison of the herein presented MCFC-based schemes with the MEA process presented by the EBTF team and previously assessed in Ref. [12] is reported in Table 7.

The integrated case shows a very low SPECCA of 0.31 MJ kg_{CO2}^{-1}, attractive not only compared to the reference value of 3.34 MJ kg_{CO2}^{-1} for MEA, but also against the value claimed by the most promising solvents (e.g., Refs. [39,41]). Instead, the non-integrated case features a SPECCA of 2.38 MJ kg_{CO2}^{-1}, a value still interesting but much closer to the figures claimed by optimized chemical solvents for post-combustion applications [42]. In terms of CO_2 removal, MCFC are not deemed to reach the very high CCR% envisaged by chemical solvent plants, due to the constraints on the minimum CO_2 concentration limit at cathode outlet; indeed, when coupled with NGCCs, MCFCs are more suitable for CO_2 removal rates close to 80%, whereas the base MEA case is designed

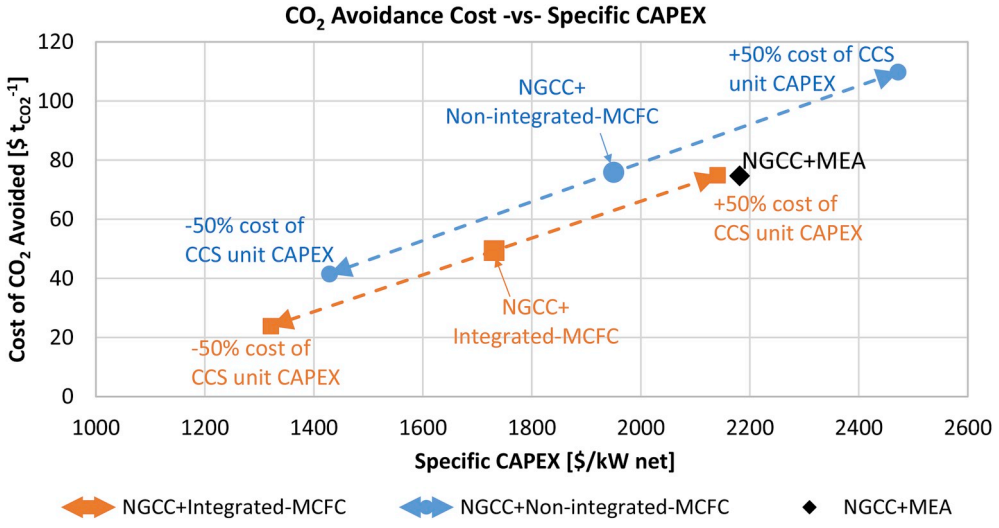

Fig. 8. Sensitivity of CCA cost of MCFC cases to specific CAPEX of the overall plant and comparison against MEA estimate.

for 90% capture.

Concerning the economic analysis, the integrated case is by far the most promising option. The base CCA of NGCC + MEA is 75 $ t_{CO2}^{-1} [12], the one for the NGCC + MCFC-non-integrated case is nearly the same (76 $ t_{CO2}^{-1}), while the one for the NGCC + MCFC-integrated case is 35% lower (49 $ t_{CO2}^{-1}) due to the lower specific investment cost (−20% compared to the MEA) and higher energy efficiency.

On the other hand, MCFC and MEA feature a different level of technological maturity, which reflects into a different level of uncertainty when evaluating their investment costs, capacity factor, and O&M costs. For this reason, since the investment cost is expected to be one of the most uncertain cost figures for the MCFC island, a sensitivity analysis was conducted to see the impact of a ±50% of the MCFC investment cost variation on the CO_2 avoidance costs. The results of this analysis are shown in Fig. 8 and indicate that the integrated scheme would feature a lower CCA even if the MCFC cost turns out to be 50% higher than assumed.

The major drawback of the integrated scheme is its unsuitability for retrofit applications: in existing NGCCs the space between the GT outlet and the HRSG inlet typically is not sufficient to host the MCFC modules. On the other hand, the non-integrated scheme seems to be suitable for retrofit applications as no modifications of the existing HRSG are expected. Only modifications of the LP and MP sections of the steam turbine should be necessary in order to accommodate the additional steam flow rate generated by the external heat exchangers. This issue is similar to that of the MEA process in which about 1/3rd of the LP steam is extracted for solvent regeneration and therefore the LP turbine should be either modified or operated in the throttling mode.

As far as operational flexibility is concerned, since high temperature MCFCs feature long start-up times, both schemes do not seem suitable for frequent on/off (cycling) operation. However, further work is necessary to assess their operational flexibility, start-up sequence and part-load performance.

In summary, the proposed integrated NGCC-MCFC scheme can achieve outstanding energy and economic performance, which considerably improves the benchmark CO_2 capture technology. A major factor is the proper matching of the MCFC temperature requirements with the similar GT outlet conditions. If the integration is not fully optimized, as is the case in the non-integrated scheme, the efficiency penalty and the increased capital costs associated to the required heat exchangers limit the advantages compared to the benchmark MEA scrubbing process.

Acknowledgment

We would like to thank the CO_2 Capture Project's Capture Team for their valuable contributions throughout the study. This work was fully funded and supported by Phase 4 of the CO_2 Capture Project (CCP). The CCP is an award-winning group of major energy companies working together to advance the technologies that will underpin the deployment of industrial-scale CO_2 capture and storage (CCS). The members of CCP's fourth phase are BP, Chevron and Petrobras.

Appendix A. Thermodynamic properties of main points in the integrated/non-integrated MCFC + NGCC cases

Integrated Case (Fig. 4)

#	G kg s^{-1}	T °C	P bar	M kmol s^{-1}	Ar	CO_2	CH_4	C_2H_6	C_3H_8	H_2O	N_2	O_2	H_2	CO
1	1165.9	15.0	1.00	40.412	0.92	0.03	-	-	-	1.03	77.3	20.7	-	-
2	1156.1	417.5	18.16	40.072	0.92	0.03	-	-	-	1.03	77.3	20.7	-	-
3	30.6	160.0	68.60	1.701	-	2.00	89.0	7.00	1.10	-	0.89	-	-	-
4	1078.0	1443.0	17.61	38.084	0.88	4.87	-	-	-	10.1	73.7	10.5	-	-
5	1321.9	610.6	1.05	46.536	0.89	3.99	-	-	-	8.43	74.4	12.3	-	-
6	1247.1	651.7	1.03	44.762	0.93	1.00	-	-	-	8.77	77.9	11.4	-	-
7	1247.1	64.3	1.00	40.380	0.93	1.00	-	-	-	8.77	77.9	11.4	-	-
8	6.2	15.0	70.00	0.342	-	2.00	89.0	7.00	1.10	0.00	0.89	-	-	-
9	18.1	300.0	1.15	0.885	-	20.5	34.4	2.71	0.43	0.00	3.84	-	26.2	11.8
10	41.5	448.1	1.15	2.185	-	8.32	13.9	1.10	0.17	59.5	1.55	-	10.6	4.78
11	126.1	651.7	1.12	4.321	-	45.0	-	-	-	46.1	0.79	-	5.50	2.65
12	126.1	124.9	1.09	4.321	-	45.0	-	-	-	46.1	0.79	-	5.50	2.65
13	12.0	96.8	22.97	0.542	-	32.2	-	-	-	0.00	5.70	-	42.8	19.3
14	78.4	32.0	110.0	1.8	-	98.3	-	-	-	0.61	0.17	-	0.30	0.56
15	23.4	565.0	1.37	1.300	-	-	-	-	-	-	-	-	-	-
16	7.1	330.8	130.00	0.392	-	-	-	-	-	-	-	-	-	-
17	7.1	87.1	127.40	0.392	-	-	-	-	-	-	-	-	-	-
18	11.2	234.5	35.00	0.621	-	-	-	-	-	-	-	-	-	-
19	11.2	25.0	34.30	0.621	-	-	-	-	-	-	-	-	-	-

Non-Integrated Case (Fig. 5)

#	G kg s^{-1}	T °C	P bar	M kmol s^{-1}	Ar	CO_2	CH_4	C_2H_6	C_3H_8	H_2O	N_2	O_2	H_2	CO
1	1330.6	86.8	1.01	46.84	0.89	3.96	-	-	-	8.38	74.38	12.39	-	-
2	1330.6	92.9	1.06	46.84	0.89	3.96	-	-	-	8.38	74.38	12.39	-	-
3	1330.4	530.0	1.05	46.83	0.89	3.95	-	-	-	8.38	74.39	12.39	-	-
4	1332.6	593.4	1.05	46.96	0.89	4.23	-	-	-	8.90	74.18	11.81	-	-
5	2.239	15.0	30.1	0.124	-	2.00	89.01	7.00	1.10	-	0.89	-	-	-
6	1332.6	580.0	1.05	46.96	0.89	4.23	-	-	-	8.90	74.18	11.81	-	-
7	1240.3	630.2	1.03	44.65	0.93	1.00	-	-	-	9.36	78.02	10.69	-	-
8	1240.3	171.4	1.02	44.65	0.93	1.00	-	-	-	9.36	78.02	10.69	-	-
9	6.7	15.0	30.1	0.374	-	2.00	89.01	7.00	1.10	-	0.89	-	-	-
10	24.6	57.1	1.11	1.175	-	23.04	28.32	2.23	0.35	-	3.98	-	28.72	13.37
11	24.6	330.0	1.09	1.175	-	23.04	28.32	2.23	0.35	-	3.98	-	28.72	13.37
12	24.6	330.0	1.09	1.175	-	23.04	28.32	2.23	0.35	-	3.98	-	28.72	13.37

(*continued on next page*)

(*continued*)

#	G kg s^{-1}	T °C	P bar	M kmol s^{-1}	Ar	CO_2	CH_4	C_2H_6	C_3H_8	H_2O	N_2	O_2	H_2	CO
13	46.6	450.0	1.09	2.396	-	11.30	13.89	1.09	0.17	50.94	1.95	-	14.09	6.56
14	138.9	630.2	1.06	4.729	-	46.41	-	-	-	41.76	0.99	-	7.27	3.57
15	22.0	95.0	1.27	1.220	-	-	-	-	-	-	-	-	-	-
16	22.0	30.0	1.31	1.220	-	-	-	-	-	-	-	-	-	-
17	138.9	283.5	1.02	4.729	-	46.41	-	-	-	81.00	0.99	-	7.27	3.57
18	138.9	30.0	1.02	4.729	-	46.41	-	-	-	41.77	0.99	-	7.27	3.57
19	17.9	80.0	1.11	0.801	-	32.86	-	-	-	0.00	5.42	-	42.12	19.60
20	22.0	114.9	1.24	1.220	-	-	-	-	-	-	-	-	-	-
21	10.0	350.0	174.6	0.554	-	-	-	-	-	-	-	-	-	-
22	10.0	100.0	174.6	0.554	-	-	-	-	-	-	-	-	-	-
23	85.4	32.0	110.	1.960	-	98.54	-	-	-	0.38	0.17	-	0.31	0.61

References

[1] I.E.A.IEA, Energy, Climate Change & Environment—2016 Insights, 2016 vol. Paris, Fra.

[2] I.P.on.C, Intergovernmental Panel on Climate Change, Climate Change 2014 Mitigation of Climate Change, Cambridge University Press, Cambridge, 2014.

[3] IPCC, Intergovernmental Panel on Climate Change, "Climate Change 2014: Impacts, Adaptation and Vulnerability, 2014.

[4] UNFCCC, United Nations framework convention on climate change united Nations, COP23 united Nations framework convention on climate change united Nations - summary for policymakers, November 2017, pp. 1–33, 2017.

[5] CaESAR, European Best Practice Guidelines for Assessment of CO2 Capture Technologies, 2011, pp. 1–112.

[6] J. Milewski, T. Wejrzanowski, Ł. Szabłowski, R. Baron, A. Szczęśniak, K. Ćwieka, Development of molten carbonate fuel cells at warsaw university of technology, Energy Procedia 142 (Dec. 2017) 1496–1501.

[7] K. Sugiura, K. Takei, K. Tanimoto, Y. Miyazaki, The carbon dioxide concentrator by using MCFC, J. Power Sources 118 (1) (2003) 218–227.

[8] I. Rexed, M. della Pietra, S. McPhail, G. Lindbergh, C. Lagergren, Molten carbonate fuel cells for CO2 separation and segregation by retrofitting existing plants - an analysis of feasible operating windows and first experimental findings, Int. J. Greenh. Gas Control 35 (2015) 120–130.

[9] G. Discepoli, G. Cinti, U. Desideri, D. Penchini, S. Proietti, Carbon capture with molten carbonate fuel cells: experimental tests and fuel cell performance assessment, Int. J. Greenh. Gas Control 9 (Jul. 2012) 372–384.

[10] H. Ghezel-Ayagh, S. Jolly, D. Patel, W. Steen, Electrochemical membrane technology for carbon dioxide capture from flue gas, Energy Procedia 108 (Mar. 2017) 2–9.

[11] ExxonMobil, FuelCell Energy trial MCFCs in carbon capture, Fuel Cells Bull. 2016 (5) (May 2016) 12–13.

[12] J. Forsyth, et al., Evaluation of five alternative CO2 capture technologies with insights to inform further development, Energy Procedia 114 (Jul. 2017) 2599–2610.

[13] E. Audasso, L. Barelli, G. Bidini, B. Bosio, G. Discepoli, Molten Carbonate Fuel Cell performance analysis varying cathode operating conditions for carbon capture applications, J. Power Sources 348 (Apr. 2017) 118–129.

[14] U.S.Department of Energy, Fuel Cell Handbook, 2004.

[15] R. Carapellucci, R. Saia, L. Giordano, Study of gas-steam combined cycle power plants integrated with MCFC for carbon dioxide capture, Energy Procedia 45 (2014) 1155–1164.

[16] P. Chiesa, S. Campanari, G. Manzolini, CO2 cryogenic separation from combined cycles integrated with molten carbonate fuel cells, Int. J. Hydrogen Energy 36 (16) (2011) 10355–10365.

[17] S. Campanari, G. Manzolini, P. Chiesa, Using MCFC for high efficiency CO2 capture from natural gas combined cycles: comparison of internal and external reforming, Appl. Energy 112 (Dec. 2013) 772–783.

[18] S. Campanari, P. Chiesa, G. Manzolini, S. Bedogni, Economic analysis of CO2 capture from natural gas combined cycles using Molten Carbonate Fuel Cells, Appl. Energy 130 (2014) 562–573.

[19] A. Amorelli, et al., An experimental investigation into the use of molten carbonate fuel cells to capture CO2 from gas turbine exhaust gases, Energy 29 (9) (2004) 1279–1284.

[20] V. Spallina, M.C. Romano, S. Campanari, G. Lozza, Application of MCFC in coal gasification plants for high efficiency CO, Volume 4, in: Cycle Innovations; Fans and Blowers; Industrial and Cogeneration; Manufacturing Materials and Metallurgy; Marine; Oil and Gas Applications, vol. 4, 2011, pp. 233–242.

[21] R. Chacartegui, B. Monje, D. Sánchez, J.A. Becerra, S. Campanari, Molten carbonate fuel cell: towards negative emissions in wastewater treatment CHP plants, Int. J. Greenh. Gas Control 19 (2013) 453–461.

[22] M. Spinelli, M.C. Romano, S. Consonni, S. Campanari, M. Marchi, G. Cinti, Application of molten carbonate fuel cells in cement plants for CO2 capture and clean power generation, Energy Procedia 63 (2014) 6517–6526.

[23] Integration of Molten Carbonate Fuel Cells in Iron and Steel Processing, Jan. 2016.

[24] R. Hill, et al., Application of molten carbonate fuel cell for CO2 capture in thermal in situ oil sands facilities, Int. J. Greenh. Gas Control 41 (2015) 276–284.

[25] S. Campanari, Carbon dioxide separation from high temperature fuel cell power plants, J. Power Sources 112 (1) (2002) 273–289.

[26] P. Greppi, B. Bosio, E. Arato, Membranes and molten carbonate fuel cells to capture CO2 and increase energy production in natural gas power plants, Ind. Eng. Chem. Res. 52 (26) (2013) 8755–8764.

[27] M. Spinelli, et al., Molten carbonate fuel cells for retrofitting postcombustion CO2 capture in coal and natural gas power plants, J. Electrochem. Energy Convers. Storage 15 (3) (2018).

[28] J. Milewski, M. Wołowicz, A. Miller, R. Bernat, A reduced order model of Molten Carbonate Fuel Cell: a proposal, Int. J. Hydrogen Energy 38 (26) (Aug. 2013) 11565–11575.

[29] P. Gabrielli, M. Gazzani, M. Mazzotti, Electrochemical conversion technologies for optimal design of decentralized multi-energy systems: modeling framework and technology assessment, Appl. Energy 221 (2018) 557–575.

[30] GS process simulation software. http://www.gecos.polimi.it/expertise/software-development/.

[31] M. Farooque, J. Daly, J. Wang, "Contaminants Control for Fuel Cells – FCE Experience, 2014.

[32] H.J. Grabke, Metal dusting of low- and high-alloy steels, Corrosion 51 (9) (1995) 711–720.

[33] D. Swanepoel, D. Kr, Rotary regenerator design theory and optimisation, Inside R & D J. 12 (3) (1996).

[34] AspenTech, Aspen Plus v8.8, Aspentech, 2016.

[35] Thermoflow, Thermoflex V. 24, 2014.

[36] M.B. Berkenpas, H.C. Frey, J.J. Fry, J. Kalagnanam, E.S. Rubin, Center for Energy and Environmental Studies, Carnegie Mellon University, Technical documentation, Integr. Environ. Control Model (May, 2009) 45–56.

[37] S. Ahmed, D. Papadias, R. Ahluwalia, T. Hua, H.-S. Roh, Performance and Cost Analysis for a 300 kW Tri-generation Molten Carbonate Fuel Cell System, 2015.

[38] CCP, Carbon Dioxide Capture for Storage in Deep Geologic Formations, vol. 4, 2015.

[39] EBTF - European Benchmark Task Force, European Best Practice Guidelines for Assessment of CO2 Capture Technologies, 2011.

[40] Carbon capture and sequestration technologies @ MIT [Online]. Available, http://sequestration.mit.edu/tools/projects/map_projects.html. (Accessed 3 May 2018).

[41] E. Sanchez Fernandez, E.L.V. Goetheer, G. Manzolini, E. Macchi, S. Rezvani, T.J. H. Vlugt, Thermodynamic assessment of amine based CO2 capture technologies in power plants based on European Benchmarking Task Force methodology, Fuel 129 (Aug. 2014) 318–329.

[42] D. Sutter, M. Gazzani, M. Mazzotti, A low-energy chilled ammonia process exploiting controlled solid formation for post-combustion CO $_2$ capture, Faraday Discuss 192 (0) (Oct. 2016) 59–83.